Journal of Materials Research and Technology 29 (2024) 4607–4621

Contents lists available at ScienceDirect

Journal of Materials Research and Technology

journal homepage: www.elsevier.com/locate/jmrt

# Development of a sprayable PVA-fiber-enhanced cement mortar with high acid-corrosion resistance for pipeline rehabilitate

Xijun Zhang [a,b,c], Mingrui Du [a,b,c], Hongyuan Fang [a,b,c,*], Xupei Yao [a,b,c], Peng Zhao [a,b,c], Xueming Du [a,b,c], Bin Li [a,b,c], Mingsheng Shi [a,b,c]

[a] School of Water Conservancy and Transportation, Zhengzhou University, Zhengzhou, 450001, China
[b] Yellow River Laboratory, Zhengzhou University, Zhengzhou, 450001, China
[c] National Local Joint Engineering Laboratory of Major Infrastructure Testing and Rehabilitation Technology, Zhengzhou, 450001, China

ARTICLE INFO

Handling editor: M Meyers

*Keywords:*
Trenchless technology
Sprayable cement mortar
PVA fiber
Mechanical properties
Acid-corrosion

ABSTRACT

The spraying method offers the advantages of environmental protection, convenient construction, and cost-effectiveness, making it widely used in pipeline structure repair. Given the complex service environment of pipelines, there is an urgent demand for high-strength and durable spraying materials. To achieve this goal, a PVA fiber reinforced cement mortar material (PFCM) with high early strength, excellent impermeability and stable acid corrosion resistance was developed through orthogonal test design. The optimal material was obtained through factors such as setting time, fluidity, compressive strength and flexural strength. The effects of the contents of fly ash, redispersible polymer powder and PVA fiber on the working and mechanical properties of the material were investigated, and further research was conducted on its tensile strength, impermeability, acid corrosion resistance. In addition, Thermogravimetric-differential Thermal Analysis (TG-DTA) was utilized to analyze the thermal stability of PFCM. X-ray diffraction (XRD) was utilized to analyze the composition of PFCM. Mercury intrusion porosimetry (MIP) was utilized to analyze the pore structure of PFCM, and the feasibility of the PFCM was verified. The results indicate that the contents of fly ash, redispersible polymer powder and PVA fiber have significant effects on the working and mechanical properties. The optimum initial setting time is 60–80 min, and the optimum fluidity is between 170 and 180 mm. The compressive strength and flexural strength of the mortar prepared with the optimum parameters are 102.5 MPa and 20 MPa, respectively. The material has an excellent spraying effect with no sagging, and exhibits high early strength, outstanding corrosion resistance, low porosity, and exceptional impermeability. This study lays the foundation for achieving high-quality spray repairs of underground drainage pipelines.

## 1. Introduction

Cement-based materials are the most commonly used artificial materials in civil engineering, with a conservative estimate of approximately 416,255 million tons of cement used annually worldwide. They find widespread applications in civil engineering [1,2], water conservancy [3–5], national defense [6,7], and various other fields. In practical engineering, the construction techniques proposed for cement-based materials include manual plastering [8], mold casting [9,10], grouting [11,12], spraying [13], and 3D printing [14].

In terms of spraying, it refers to spraying the prepared cement-based materials onto the surface of rock or concrete [15–17]. A representative application of sprayed cement-based materials includes shotcrete technology for constructing tunnel lining structure [18]. Another example is the cement mortar spray lining technology used to reinforce underground drainage pipes [19,20].

As shown in Fig. 1, it refers to using the centrifugal force generated by the high-speed rotation of the pneumatic rotary nozzle to evenly and continuously spray the prepared high-performance cement-based lining slurry onto the inner wall of the pipeline or inspection well to be repaired. Simultaneously, the rotary nozzle is suspended by a lifting arm, moving back and forth within the pipeline or well. This process results in the creation of a uniform, continuous, and dense lining on the inner surfaces of the pipeline or well, ultimately achieving structural repair (as shown in Fig. 1). This technology offers several advantages, including high efficiency, a short cycle, no disruption to traffic,

* Corresponding author. School of Water Conservancy and Transportation, Zhengzhou University, Zhengzhou, 450001, China.
*E-mail address:* 18337192244@163.com (H. Fang).

https://doi.org/10.1016/j.jmrt.2024.02.144
Received 9 December 2023; Received in revised form 13 February 2024; Accepted 19 February 2024
Available online 22 February 2024

environmental friendliness, low overall cost, and enhanced safety [21,22]. It constitutes an integral component of the trenchless repair technology system for underground pipelines and has found widespread application in the restoration of corroded pipelines [23,24].

For in-situ spraying repair technology, the performance of cement mortar is the key to long-term reinforcement effect. Due to long-term microbial erosion on the inner wall of underground drainage pipelines, the upper part of the earth pressure and vehicle load, the geological conditions are unclear, resulting in a decrease in pipeline bearing capacity and the actual service environment is extremely complicated [25,26]. Nowadays, with the continuous acceleration of the urbanization process, the scale of the city will continue to expand, and the transformation of the urban drainage network will also be a long-term sustained systematic project. Trenchless spray repair technology is increasingly popular [21], but there are stringent requirements for the early strength, fluidity, sprayability and durability of repair materials, particularly when dealing with acid-resistant media. Early high strength ensures that the repaired pipeline can be swiftly reintegrated into service, while high fluidity and excellent sprayability ensure uniformity in the sprayed repair layer. Acid corrosion resistance and high impermeability are crucial in preventing future cracks or damage caused by acid corrosion or ion erosion, enhancing the long-term effectiveness of the repair [27]. Traditional mortar repair methods exhibit shortcomings such as uneven application, cracking, and peeling, making it imperative to develop high-performance sprayed cement mortar that aligns with practical needs. Zhao et al. [28] employed an organic silane fly ash (FA) hybrid and a polyethylene pyrrolidone (PVP) cross-linking network to enhance the compressive strength of polymer-modified cementitious materials. According to the results of nanoindentation testing, the micro-mechanical properties of the cement slurry were significantly improved, and the pore structure exhibited marked enhancement in the mercury intrusion porosimetry results. Gobel et al. [29]modified the bonding material by adding polymers to improve durability and bonding strength. Ryu et al. [30] conducted an experimental study on the properties of PVA fiber-reinforced cement--based composites as repair materials. The results indicate that not only the bearing capacity is significantly improved, but also the ductility is enhanced without any interface failure or brittle fracture. Mishra et al. [31]studied the mechanical properties of graphene oxide modified cement mortar materials and their effects on the hydration mechanism of cement slurry and carbonate mineralization. This discovery indicates that the application of GO not only improves the mechanical properties of the cement system, but also significantly enhances $CO_2$ storage in the cement system. In terms of improving the ordinary cementitious materials performance, methods proposed by previous researchers include polymer modified cementitious materials [28,29], fiber reinforced cementitious materials [32], and graphene oxide modified cementitious materials [33,34]. Among them, fiber reinforced cementitious materials have the characteristics of lightweight, high-strength, and high tough, making them more widely used.

Based on this, in order to develop a fiber reinforced cement mortar material suitable for spraying technology with early strength, high strength, good durability and excellent sprayability, the optimal ratio of the material was designed through orthogonal test. The Thermogravimetric-differential Thermal Analysis (TG-DTA) and Mercury Intrusion Porosimetry (MIP) experiments were used. Verify whether the material has good thermal stability, impermeability and acid corrosion resistance. This relevant research provides a foundation for achieving high-quality repairs of underground drainage pipelines.

## 2. Experimental procedures

### 2.1. Raw materials, mixing designs and preparation of fresh PFCM

The bind materials used here was ordinary Portland cement (OPC, type P.O.52.5) silica fume (SF), fly ash (FA), which are respectively from Henan Mengdian Group, Wuhan Sinocem Smartec Co., Ltd and Henan Borun Casting Materials Co., Ltd. SF can effectively prevent the intrusion and corrosion of acid ions, while FA was used to enhance the sustainability and fluidity of the PVA-fiber-reinforced cement mortar composition. The quartz sand (QS) and a quartz powder (QP) were used as fine aggregate. The particle size and morphologies of the bind materials were analyzed using the Malvern laser particle size instrument and scanning electron microscope (SEM), and the results are shown in Figs. 2 and 3. Redispersible polymer powder (RDP), hydroxypropyl methylcellulose, calcium formate, and a commercially available defoamer were added to enhance constructability and adhesion. The fiber reinforcements used in PVA-fiber-reinforced cement mortar were ultra-high-strength polyvinyl

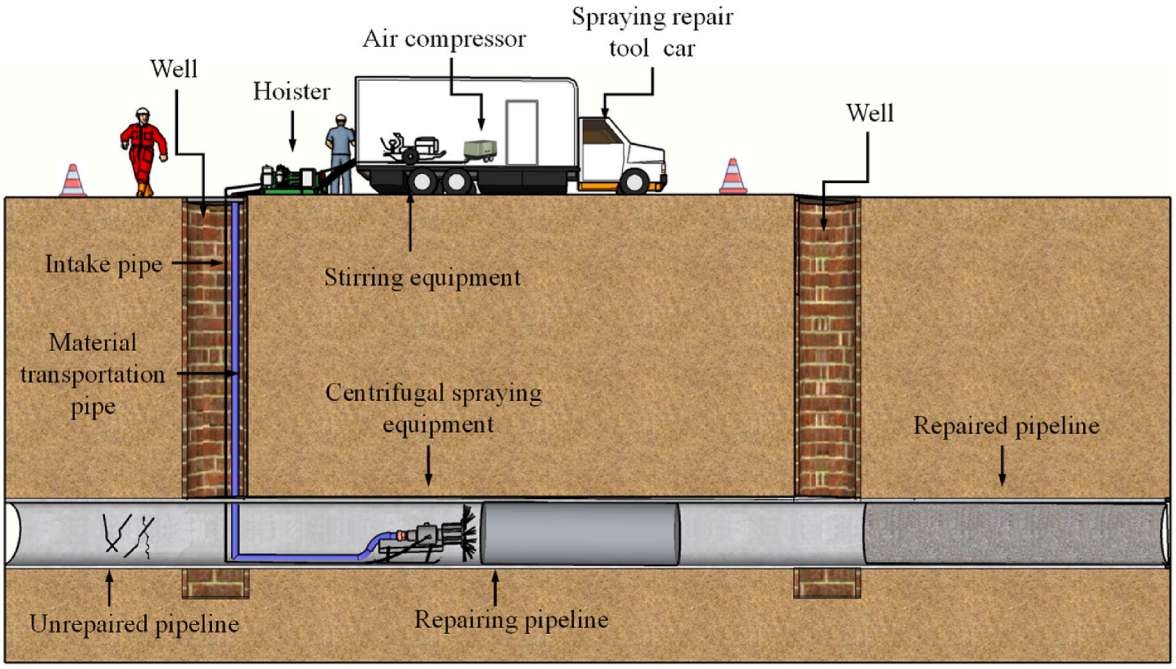


**Fig. 1.** Mortar spraying repair pipeline diagram.

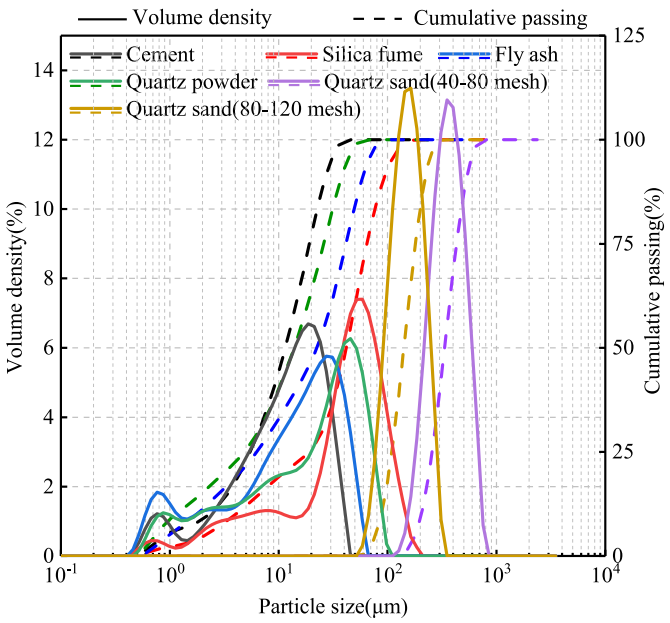


**Fig. 2.** Particle size distributions of raw materials.

alcohol (PVA) fibers (Fig. 4), with a length of 6 mm and a diameter of 14 μm. The PVA fibers have 35 GPa elastic modulus and 1200 MPa tensile strength. The chemical composition of the raw material in Table 1.

### 2.2. Preparations of PFCM and testing methods

A high-range water reducer (HRWR, PCA®-400P) was incorporated at a 0.3% weight of the binder. Silica fume possesses highly active volcanic ash properties, can react with calcium hydroxide, and has very small particle sizes that can fill small pores in mortar. Therefore, it is widely used in ultra-high-performance mortar materials. Sprayed mortar demands extremely high sagging resistance, with moderate fluidity required. Due to the significant influence of silica fume content on mortar fluidity, the fluidity is initially adjusted using silica fume. The final choice is to maintain silica fume at 7% of the cementitious material. Subsequently, for the three influencing factors of fly ash, redispersible polymer powder, and PVA fiber, the optimal mixing ratios were determined using orthogonal experimentation [35,36]. Three levels were considered for each factor: the replacement rate of fly ash to cement at 5, 10, and 15 %; the mass dosage of redispersible polymer powder at 1, 2, and 3 %; and the volume fraction of PVA fiber at 0.1, 0.3, and 0.5 %. The experimental factor level table is shown in Table 2, and the specific proportions of composite materials are listed in Table 3.

To prepare specimens, all dry ingredients (OPC, SF, FA, QS, RDP, and QP) were mixed in a 5-L mortar mixer at 140 rpm for 3 min. The PVA fibers was then added to the dry ingredients which were mixed for 6 min at 140 rpm to ensure sufficient blending of PVA fibers. The water premixed with HRWR was then added to the composite mixture which were mixed for 6 min at 285 rpm. The fluidity and setting time of the fresh PFCM were experimentally tested using NLD-3 electric flow table and SZ-100 digital display setting time tester according to methods proposed in Standard Specification for Flow Table for Use in Tests of Hydraulic Cement [37]and Standard for Test Method of Basic Properties of Construction Mortar [38].

The compressive strength was measured using 70.7-mm cubes following JGJ/T 70–2009 (Fig. 5a) [38]. The test employed a WHY-2000 type electro-hydraulic servo testing machine with a loading rate of 1.5 kN/s, and three identical cubes were tested for each mixture. All blocks were cured for 3 days, 7 days, and 28 days under standard curing conditions of 20 ± 2 °C and humidity above 95%. Similarly, the flexural strength was measured using 40 × 40 × 160 rectangular samples (Fig. 5b). The WHY-300/10 type electro-hydraulic servo testing machine was used, with a loading rate of 50 N/s. The optimal ratio was selected based on testing the compressive and flexural strength. For the optimal group, a direct tensile test was conducted using three dog-bone-shaped specimens (Fig. 5c). After curing for 3 days, 7 days, and 28 days in a standard curing room (20 ± 2 °C, 90 ± 5% RH), the INSTRON 5982 electronic universal material testing machine was employed for direct tensile testing at a rate of 0.5 mm/min. Deformation was measured using an extensometer. The direct tensile test device was arranged as shown in Fig. 6, and the end of the specimen was sequentially reinforced with carbon fiber cloth and aluminum sheet to prevent concentrated stress resulting from the force of the testing machine, which could lead to end failure.

The material composition of the mortar is analyzed using X-ray diffraction (XRD). This involves primarily grinding the mortar into powder. The testing range is 5–90°, the scanning speed is 2°/min, and the scanning step length is 0.02°.

**Fig. 4.** Photograph of polyvinyl alcohol (PVA) fibers.

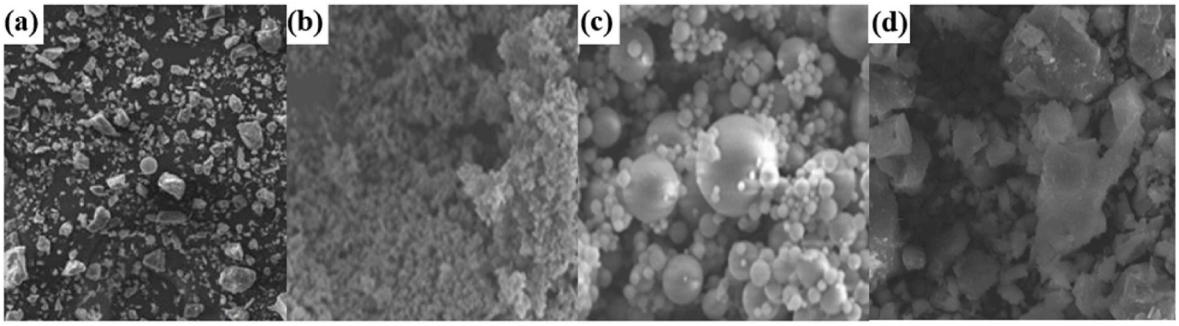


**Fig. 3.** SEM images of (a) Portland cement, (b) silica fume, (c) fly ash and (d) quartz sand.

**Table 1**
The chemical composition of the raw material.

| Type | CaO | Al2O3 | SiO2 | Fe2O3 | MgO | K2O | SO3 | Cl-1 | TiO2 | Na2O | P2O5 |
|---|---|---|---|---|---|---|---|---|---|---|---|
| OPC | 62~67 | 4~7 | 20~24 | 2.5–6.0 | 3.5 | – | – | – | – | – | – |
| SF | 0.16 | 0.32 | 99.23 | – | 0.12 | 0.15 | 0.62 | 0.009 | – | – | – |
| FA | 3~4 | 24~25 | 62~63 | 4~5 | 1~2 | – | 0.1–1 | – | 1~2 | 0.1–0.5 | 0.2–0.4 |

**Table 2**
The orthogonal experiment factor level table.

| Levels | Factors | | |
|---|---|---|---|
| | A<br>Fly ash content/% | B<br>Redispersible polymer powder content/% | C<br>PVA fiber content/% |
| 1 | 5 | 1 | 0.1 |
| 2 | 10 | 2 | 0.3 |
| 3 | 15 | 3 | 0.5 |

### 2.3. Sprayability, impermeability, and acid-corrosion resistance characterizations

Based on the test results of fluidity, setting time, and basic mechanical properties, the optimal ratio for the cement mortar was determined. Subsequently, further spraying tests were conducted to assess its sprayability. The equipment and process used are as follows.

The centrifugal spraying equipment M/P–80W was developed by Wuhan CUG Trenchless Technology Research Institute. This equipment consists of a pneumatic rotary injector, mortar spraying machine, air compressor, generator, and other components. The nozzle is circular and features a single hole at its base for the inlet of compressed air (as shown in Fig. 7). The entire process takes place indoors, with all-round pipes positioned indoors. The distance from the nozzle outlet to the pipe wall is 197.5 mm, and the nozzle discharge port is perpendicular to the pipe wall for spraying.

Impermeability tests and chloride ion penetration tests were conducted to verify the impermeability characteristics of the PFCM. In the next test, mortar powder is prepared. Thermal analysis is employed to quantitatively determine reaction products, and the sample is analyzed in a platinum pot. The analyzer is heated at a rate of 10 °C/min, starting from room temperature and reaching 1000 °C. Nitrogen is used as the protective gas.

To investigate the influence of acidic solutions on the mechanical properties of sprayed mortar, a long-term accelerated corrosion test was conducted in the laboratory. A specific quantity of 98% concentrated sulfuric acid was prepared to create acid solutions with a pH of 2. To accelerate the corrosion rate, the pH value of the solution was monitored daily to maintain a constant pH value. The samples were subjected to corrosion for 0 days, 3 days, 7 days, 28 days, 56 days, 112 days, and 180 days, respectively. The quality of the samples before and after corrosion was assessed, and compression tests and three-point bending tests were performed. The average flexural strength, compression test results, and average elastic modulus of each group of specimens were recorded.

Additionally, the AutoPore V 9600 mercury injection instrument, manufactured by Micromeritics in the United States, was employed to assess the pore structure characteristics of the samples with varying corrosion cycles. This assessment included pore distribution, average pore size, maximum pore size, maximum pore size, and porosity. The calculation of hole diameter and volume for different small holes primarily relies on the functional relationship between the amount of mercury pressed into the porous system and the pressure. The instrument features a mercury contact angle of 130° and a mercury surface tension of 485 dyn/cm. Before conducting the mercury injection test, the sample to be tested was initially soaked in absolute ethanol for more than 48 h to halt hydration and dehydration. Subsequently, the sample was removed and dried in an oven at 60 °C until it reached a constant weight. Finally, the dried sample was allowed to cool in a dryer for the MIP test.

## 3. Results and discussions

### 3.1. Working performance

The setting times of fresh PFCM with nine different mixing designs are illustrated in Fig. 8. When the content of redispersible polymer powder is 2%, the mortar exhibits relatively short setting times, with the shortest initial setting time at 30 min and the shortest final setting time

**Table 3**
Mixing ratio of spray mortar (g).

| Number | Mixture | OPC | SF | FA | QP | QS (40–80 mesh) | QS (80–120 mesh) | PVA | RDP | Water |
|---|---|---|---|---|---|---|---|---|---|---|
| 1 | F5V1P0.1 | 782 | 71 | 46 | 90 | 465 | 310 | 1.14 | 9 | 198 |
| 2 | F5V2P0.5 | 782 | 71 | 46 | 90 | 465 | 310 | 6 | 18.4 | 198 |
| 3 | F5V3P0.3 | 782 | 71 | 46 | 90 | 465 | 310 | 3.6 | 26.9 | 198 |
| 4 | F10V1P0.5 | 738 | 71 | 90 | 90 | 465 | 310 | 6 | 9 | 198 |
| 5 | F10V2P0.3 | 738 | 71 | 90 | 90 | 465 | 310 | 3.6 | 18.4 | 198 |
| 6 | F10V3P0.1 | 738 | 71 | 90 | 90 | 465 | 310 | 1.14 | 26.9 | 198 |
| 7 | F15V1P0.3 | 692 | 71 | 136 | 90 | 465 | 310 | 3.6 | 9 | 198 |
| 8 | F15V2P0.1 | 692 | 71 | 136 | 90 | 465 | 310 | 1.14 | 18.4 | 198 |
| 9 | F15V3P0.5 | 692 | 71 | 136 | 90 | 465 | 310 | 6 | 26.9 | 198 |

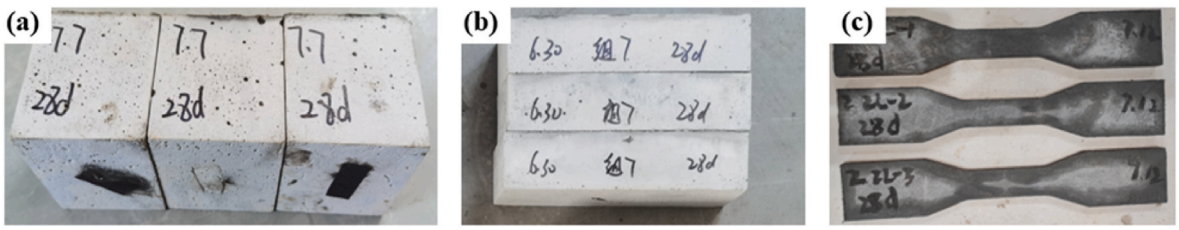


**Fig. 5.** Test Specimen:(a) 70.7 × 70.7 × 70.7 mm, (b) 160 × 40 × 40 mm, and (c) dog-bone shaped molds.

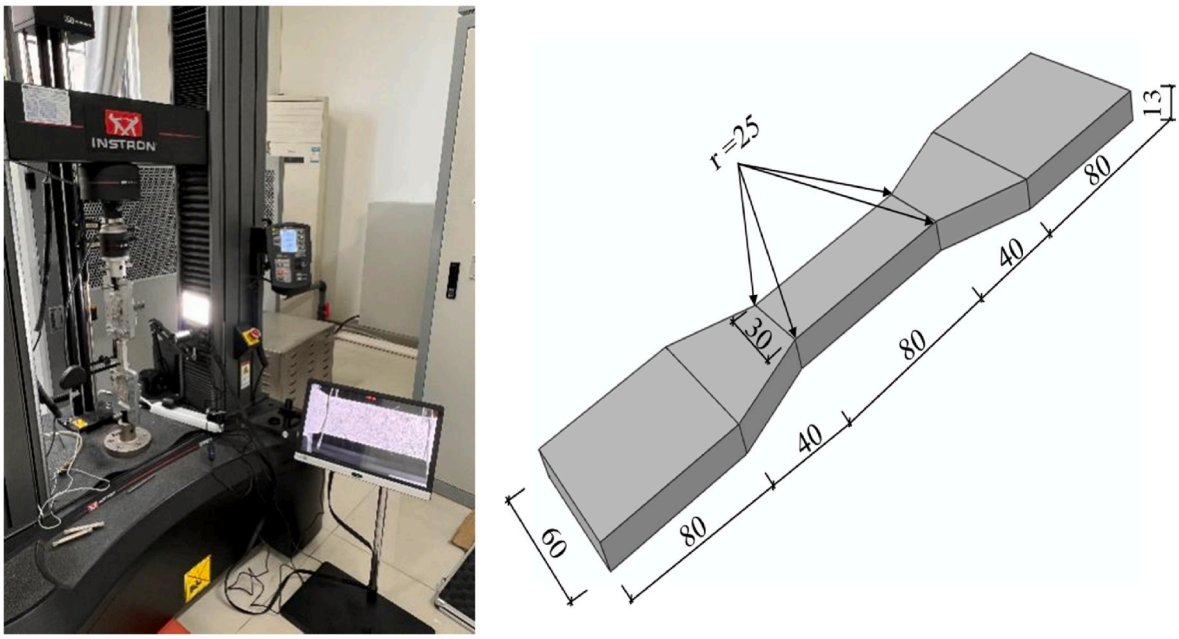


**Fig. 6.** The direct tensile test device and specimen dimensions (unit:mm).

**Fig. 7.** Pneumatic rotary sprayer.

at 90 min. Conversely, when the fly ash content is 5%, the setting time is the shortest. However, when the fly ash content is 15%, the setting time is the longest. According to previous studies, different fineness of fly ash has different setting time for mortar materials, some fly ash extends the setting time, and some fly ash shortens the setting time. For example, Choi et al. [39] replaced Portland cement with Blaine fineness of 4125 $cm^2/g$ (40F), 6686 $cm^2/g$ (60F) and 9632 $cm^2/g$ (90F). The replacement ratios were 0 (which was the control mix), 15, 30, 45 and 60% by binder mass, respectively. The test results showed that the setting time of the fly ash mixes where 15 and 30% of the cement was replaced with fine fly ashes was faster than that of the control mix. However, Tong et al. [40] discussed the effect of large amount of fly ash on the setting time of cement fly ash grout through laboratory tests and found that with the increase of fly ash content, the setting time of grout extended. In this study, only primary fly ash is used, and the conclusion is consistent with Tong. The increase of fly ash content can prolong the setting time of mortar. This indicates that the addition of a certain amount of redispersible polymer powder, coupled with a reduction in the amount of fly ash, is beneficial for shortening the setting time.

Tables 4 and 5 analyze the range and variance of the orthogonal test results. The influencing factors on the initial setting time are ranked from the largest to the smallest: fly ash > PVA fiber > redispersible polymer powder. The weight of the influencing factors affecting the final setting time is the same as for the initial setting time. The combination with relatively short initial and final setting times is $A_3B_3C_1$. The significance of the variance analysis indicates that fly ash has the highest significance, followed by redispersible polymer powder and PVA fiber, and these results consistent with the range analysis.

To further investigate the effects of fly ash content, redispersible polymer powder content, and PVA fiber content on setting time, a curve of setting time variation under the influence of various factors was established, as shown in Fig. 9. From Fig. 9 (a), it can be seen that the initial and final setting times increase with the increase of fly ash content. The setting time is the shortest at 5% fly ash content, with initial and final setting times of 30 min and 135 min, respectively. However, the setting time of mortar with 15% fly ash content is the longest, with initial and final setting times 4.5 and 1.6 times the setting time of 5% fly ash content, respectively. From Fig. 9 (b), it can be observed that the addition of redispersible polymer powder from 1% to 2% significantly reduces the setting time, while an increase in the addition from 2% to 3% leads to a significant increase in the setting time. However, the setting time is still shorter than that of the mixture with a content of 1%. Nan et al. [41] indicates that polymer modified fast hardening cement mortar is widely used in repair materials because of its short setting time. From Fig. 9 (c), the initial setting time shows a trend of slowly decreasing first and then significantly decreasing with the increase of PVA fiber content. The final setting time shows a linear decreasing trend with the increase of PVA fiber content. This can be attributed to the

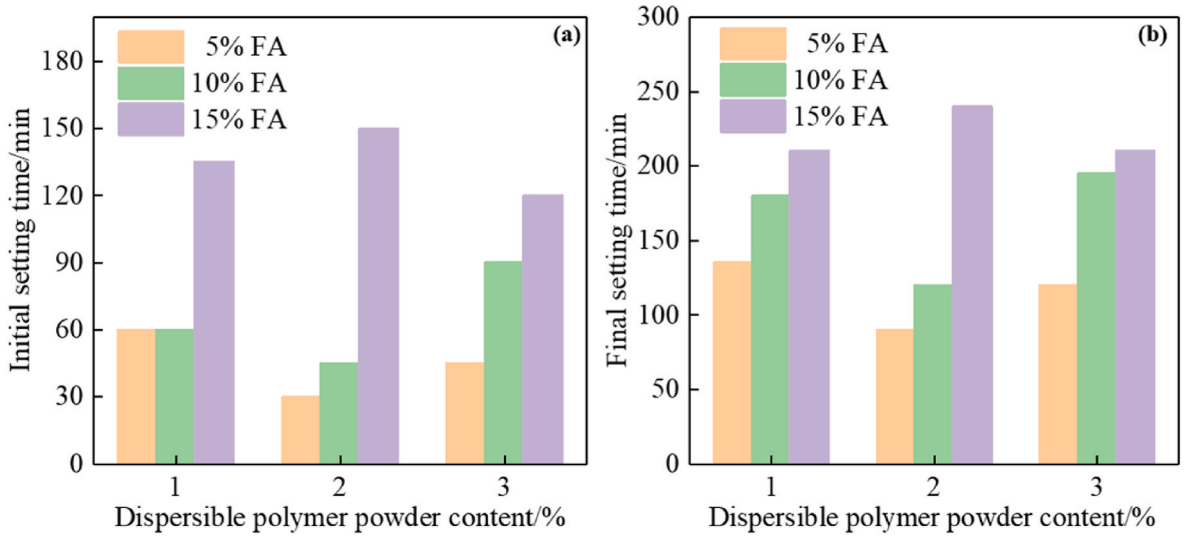


**Fig. 8.** Setting time of nine groups of mortar samples in orthogonal test: (a) initial setting time, (b) final setting time.

**Table 4**
Range analysis of mortar setting time.

| Setting time | Level | A.FA (%) | B.RDP (%) | C.PVA (%) |
|---|---|---|---|---|
| Initial setting (min) | K1 | 45 | 85 | 100 |
| | K2 | 65 | 75 | 75 |
| | K3 | 135 | 85 | 70 |
| | R | 90 | 10 | 30 |
| Final setting (min) | K1 | 115 | 175 | 190 |
| | K2 | 165 | 140 | 150 |
| | K3 | 220 | 175 | 160 |
| | R | 105 | 25 | 40 |

presence of hydroxyl inside PVA fibers, which have hydrophilicity. The absorption of free water increases the effective concentration of alkaline activators and further shortens the setting time, which is consistent with the report by Lu et al. [42]. From this, it can be seen that choosing low fly ash content and high PVA fiber content has a beneficial effect on shortening the setting time.

According to the fluidity test method, use a caliper to measure the vertical and horizontal length of the mixture passing through the center of the circle after paving each group of mix proportion specimens. Take the average value as the fluidity of this group of mix proportion, and summarize the test results in Table 6.

Tables 7 and 8 analyzes the range and variance of the orthogonal test results for fluidity. The influencing factors of the fluidity are sorted from large to small: fly ash > PVA fiber > redispersible polymer powder. Using SPSSAU to perform three factors variance analysis, through comparing the F value, the impact of various factors on fluidity. The ranking order from largest to smallest is consistent with range analysis. The variance analysis is different from range analysis in that it cannot analyze whether factors can enhance or weaken experimental

**Table 5**
Variance analysis of mortar setting time.

| Setting time | Level | Square sum | *df* | Mean square | *F* | *p* | Significance |
|---|---|---|---|---|---|---|---|
| Initial setting | A.FA(%) | 13400 | 2 | 6700 | 67.000 | 0.015 | * |
| | B.RDP(%) | 200 | 2 | 100 | 1.000 | 0.500 | – |
| | C.PVA(%) | 1550 | 2 | 775 | 7.750 | 0.114 | – |
| Final setting | A.FA(%) | 2600 | 2 | 1300 | 2.737 | 0.268 | – |
| | B.RDP(%) | 16550 | 2 | 8275 | 17.421 | 0.054 | – |
| | C.PVA(%) | 1250 | 2 | 625 | 1.316 | 0.432 | – |

*$p < 0.05$ **$p < 0.01$.

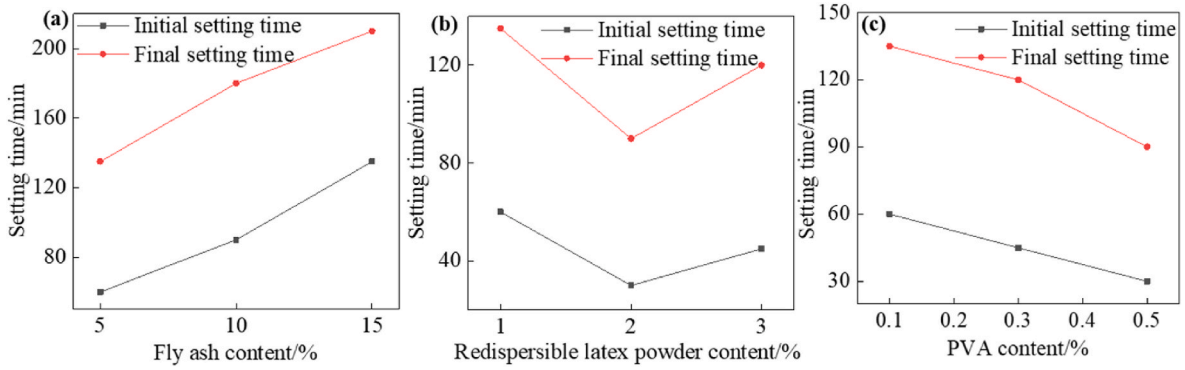


**Fig. 9.** Influence of different factors on mortar setting time.

indicators. However, it can be compared with a defined value at a given level of significance to determine whether factors have a significant impact on experimental values. The significance of variance analysis shows that fly ash has the highest significance, followed by redispersible polymer powder and PVA fiber, and the results are consistent with the range analysis results.

From Fig. 10, it can be seen that the fluidity range among various influencing factors in mortar ranges from large to small as fly ash, PVA fiber, and redispersible polymer powder. This indicates that among these three influencing factors, fly ash has the greatest impact on the fluidity of mortar, followed by PVA fiber, and finally redispersible polymer powder. In addition, fly ash also has a positive effect on improving fluidity, which is consistent with the results of Li et al. [43]. PVA fibers and redispersible polymer powder have a negative effect on fluidity, reducing the material fluidity [44,45].

### 3.2. Mechanical properties

The compressive test results are shown in Fig. 11. It can be seen that the compressive strength at 3, 7, or 28 days is the best for the fourth group, with a strength of 80 MPa at 3 days. This material greatly improves the early strength of the pipeline spraying material. From Table 9 and Fig. 11, it can be seen that the range values of various influencing factors in the 28d compressive strength are in descending order: redispersible polymer powder > fly ash > PVA fiber, indicating that these three influencing factors have the greatest impact on the compressive strength of mortar, with redispersible polymer powder followed by fly ash and PVA fiber [46,47]. Further determine the optimal mix ratio as $A_2B_1C_3$. By comparing the F-values in Table 10 with the variance analysis, the influence of various factors on the compressive strength of mortar can be obtained. The order from largest to smallest is consistent with the range analysis, but for a given significance level of $p < 0.05$, these three influencing factors do not have a significant impact. Fly ash, redispersible polymer powder, and PVA fiber have little effect on the compressive strength of PFCM.

From Fig. 12, with the increase of fly ash content, the 28d compressive strength of the mortar first significantly increased and then slowly increased. The addition of 15% fly ash resulted in a 10.2% increase in mortar compressive strength, indicating that fly ash positively influences compressive strength [48]. On the other hand, as the content of redispersible polymer powder increases, the compressive strength of the mortar significantly decreased by 5.6% and 12.2%, respectively [49]. Additionally, as the amount of PVA fiber added increases, the compressive strength initially shows an upward trend, followed by a decrease, ultimately stabilizing [50].

The flexural test results are shown in Fig. 13. From the figure, it can be seen that the flexural strength of the second and fourth groups at 28 days reaches 20 MPa, and the early strength can also reach around 16 MPa, indicating a high flexural strength. From Table 11 and Fig. 13, the range values of the three factors affecting the 28-day flexural strength of the mortar vary in descending order: fly ash > redispersible polymer powder > PVA fiber. This suggests that fly ash has the most significant impact on flexural strength, followed by redispersible polymer powder and PVA fiber [51]. Based on the degree of influence shown in Table 11, the optimal factor level is selected as $A_1B_2C_3$. By comparing the F-values in Table 12 with the variance analysis, it can be concluded that the influence of various factors on the flexural strength of mortar is in the order of fly ash > PVA fiber > redispersible polymer powder, from highest to lowest. However, for a given significance level of $p < 0.05$, none of these three influencing factors have a significant impact. Fly ash, redispersible polymer powder, and PVA fiber have little effect on the flexural strength.

The flexural strength first slowly decreases and then sharply decreases with the increase of fly ash content, with a maximum decrease of 7.5% [52]. As the amount of redispersible polymer powder increases, it shows a trend of first increasing and then decreasing [53]. However, with the increase of PVA fiber content, the flexural strength first slowly increases and then significantly increases (see Fig. 14). PVA fibers have significantly improved flexural strength [54].

Fig. 15 displays the XRD patterns of nine groups of samples with varying ratios. The diffraction peaks of different components in samples with different ratios exhibit similarity, indicating the presence of identical hydration products. The primary diffraction peaks observed include silica and ettringite [55], along with traces of calcium carbonate, calcium hydroxide, and a small quantity of gypsum. Notably, the diffraction peak intensity of silica is the highest, suggesting that silica does not actively participate in the hydration reaction. The generation of calcium hydroxide results from both the hydration reaction of $C_2S$ and $C_3S$, as well as a certain amount of calcium hydroxide produced by fly ash itself.

**Table 6**
Fluidity table of orthogonal test.

| Number | Factor & Level | | | Fluidity (mm) |
|---|---|---|---|---|
| | A.FA (%) | B.RDP (%) | C.PVA (%) | |
| 1 | 5 | 1 | 0.1 | 165 |
| 2 | 5 | 2 | 0.5 | 125 |
| 3 | 5 | 3 | 0.3 | 140 |
| 4 | 10 | 1 | 0.5 | 175 |
| 5 | 10 | 2 | 0.3 | 155 |
| 6 | 10 | 3 | 0.1 | 185 |
| 7 | 15 | 1 | 0.3 | 200 |
| 8 | 15 | 2 | 0.1 | 225 |
| 9 | 15 | 3 | 0.5 | 193 |

**Table 7**
Range analysis of mortar fluidity.

| Level | A.FA (%) | B.RDP (%) | C.PVA (%) |
|---|---|---|---|
| K1 | 143.33 | 180 | 191.67 |
| K2 | 171.67 | 168.33 | 165 |
| K3 | 206 | 172.67 | 164.33 |
| R | 62. 67 | 11. 67 | 27.33 |

**Table 8**
Variance analysis of mortar fluidity.

| Level | Square sum | *df* | Mean square | *F* | *p* | Significance |
|---|---|---|---|---|---|---|
| A.FA(%) | 5908 | 2 | 2954 | 32.465 | 0.030 | * |
| B.RDP (%) | 209 | 2 | 104 | 1.147 | 0.466 | – |
| C.PVA (%) | 1458 | 2 | 729 | 8.015 | 0.111 | – |

*$p < 0.05$ **$p < 0.01$.

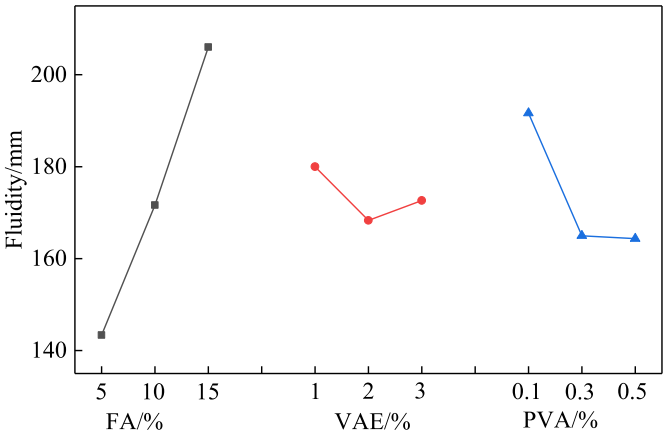


**Fig. 10.** Horizontal relationship between fluidity *K* and various factors.

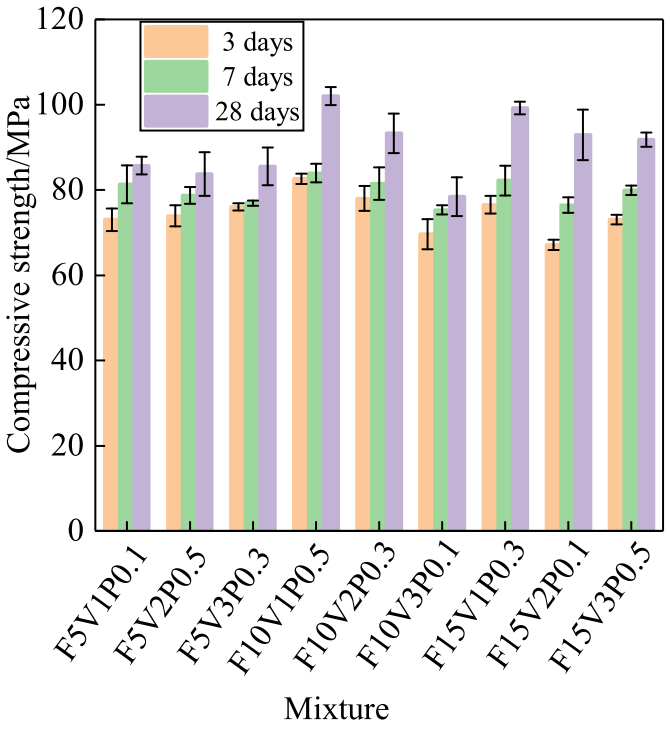


**Fig. 11.** Compressive performance test results.

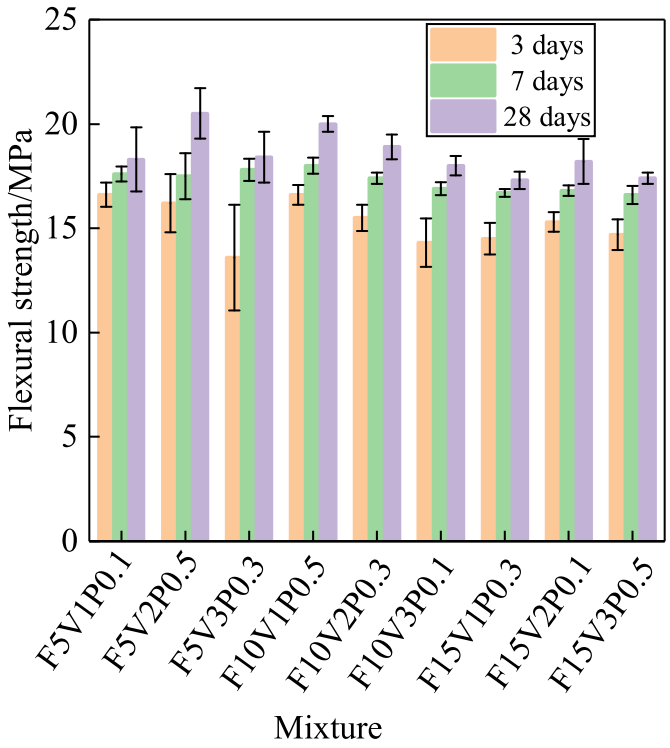


**Fig. 13.** Flexural performance test results.

**Table 9**
Range analysis of mortar compressive strength.

| Level | A.FA (%) | B.RDP (%) | C.PVA (%) |
|---|---|---|---|
| K1 | 84.97 | 95.63 | 85.67 |
| K2 | 94.63 | 89.97 | 92.5 |
| K3 | 91.23 | 85.23 | 92.67 |
| R | 9.67 | 10.4 | 7 |

**Table 10**
Variance analysis of mortar compressive strength.

| Level | Square sum | *df* | Mean square | *F* | *p* | Significance |
|---|---|---|---|---|---|---|
| A.FA(%) | 144.276 | 2 | 72.138 | 2.373 | 0.296 | – |
| B.RDP(%) | 162.676 | 2 | 81.338 | 2.675 | 0.272 | – |
| C.PVA(%) | 95.722 | 2 | 47.861 | 1.574 | 0.388 | – |

$^{*}p < 0.05$ $^{**}p < 0.01$.

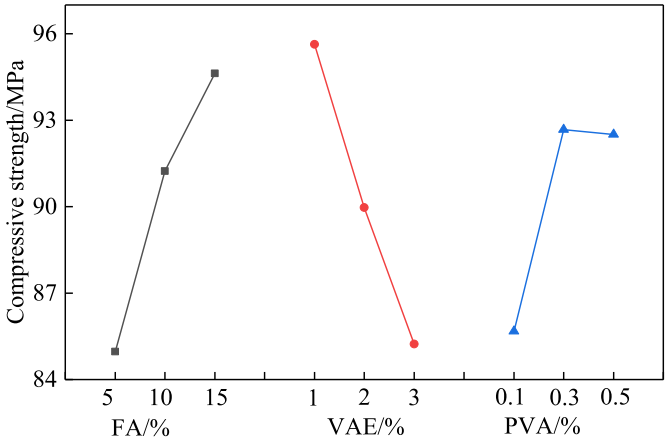


**Fig. 12.** Horizontal relationship between compressive strength *K* and various factors.

**Table 11**
Range analysis of mortar flexural strength.

| Level | A.FA (%) | B.RDP (%) | C.PVA (%) |
|---|---|---|---|
| K1 | 19.07 | 18.53 | 18.17 |
| K2 | 18.97 | 19.2 | 18.2 |
| K3 | 17.63 | 17.93 | 19.3 |
| R | 1.43 | 1.27 | 1.13 |

**Table 12**
Variance analysis of mortar flexural strength.

| Level | Square sum | *df* | Mean square | *F* | *p* | Significance |
|---|---|---|---|---|---|---|
| A.FA(%) | 3.842 | 2 | 1.921 | 5.687 | 0.15 | – |
| B.RDP(%) | 2.409 | 2 | 1.204 | 3.566 | 0.219 | – |
| C.PVA(%) | 2.496 | 2 | 1.248 | 3.694 | 0.213 | – |

$^{*}p < 0.05$ $^{**}p < 0.01$.

The hydration of tricalcium aluminate produces hydrated calcium aluminate, and gypsum reacts with hydrated calcium aluminate to form hydrated calcium sulfoaluminate needle shaped crystals (ettringite). The presence of calcium carbonate facilitates the reaction between calcium ions and gypsum, leading to the formation of ettringite [56,57].

### 3.3. Determination of the mixing design

Based on the analysis of setting time, fluidity, compressive strength, and flexural strength, it is essential for engineering repair mortar to have a setting time that is neither too long nor too short, as this can affect the construction process. After analyzing compressive and flexural strength, the optimal proportions were found in the second group ($A_1B_2C_3$) and the seventh group ($A_3B_1C_2$), both of which exhibited setting times that were either too long or too short. The fourth group ($A_2B_1C_3$), with initial and final setting times of 60 min and 180 min, respectively, demonstrated moderate setting times. Additionally, its 28-day compressive strength and flexural strength were comparable to those of the second

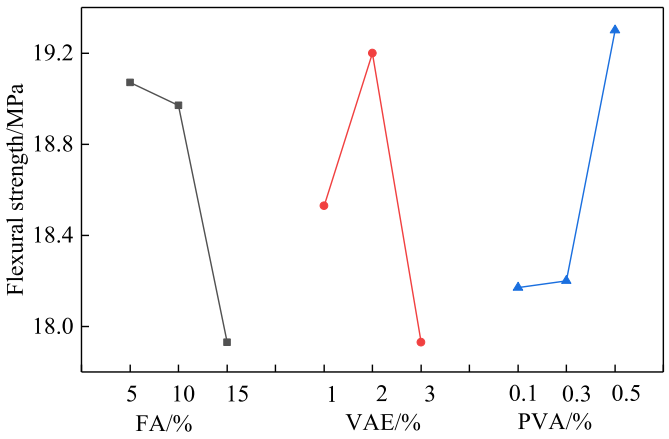


**Fig. 14.** Horizontal relationship between flexural strength *K* and various factors.

and seventh groups, while also offering better early strength and fluidity, making it suitable for use in sprayed concrete applications. Therefore, based on orthogonal experimental analysis, the optimal ratio is $A_2B_1C_3$, which corresponds to 10% fly ash content, 1% redispersible polymer powder content, and 0.5% PVA fiber content. Subsequent studies will be conducted using this ratio as the standard.

### 3.4. Sprayability

The examination of the PFCM is carried out using centrifugal spraying equipment. As depicted in Fig. 16, the material sprayed from the nozzle adheres completely to the inner wall of the pipeline in the form of dispersed particles, thanks to the centrifugal force generated by high-speed rotation. Importantly, this material does not suffer from wastage due to dripping. In the context of spraying, materials do not need to flow solely under the influence of gravity. However, materials with limited deformation capacity can impede the sprayability and potentially lead to nozzle blockages and inadequate atomization. In our experiment, PVA fiber was employed. Given that PVA fiber is a hydrophilic fiber known for its strong adhesion to substrates, the material achieves a balance between effective atomization and ease of construction during the spraying process [58]. Furthermore, in vertical spraying, the material can reach a thickness of 30 mm without any issues of dripping, shedding, or excessive flow (as shown in Fig. 16), indicating excellent sprayability.

### 3.5. Tensile strength

A direct tensile test was conducted on the selected mix proportion materials. This test was conducted using the INSTRON 5982 electronic universal material testing machine from the American ITW Group's Instron Corporation [59], and the tensile specimens were dumbbell shaped. As shown in Fig. 17, this material still has high early tensile strength, with a 3 day tensile strength of 4.83 MPa, which has reached 84.7% of the 28 day strength.

Research on the tensile properties of PVA fiber-reinforced mortar reveals that the tensile failure does not occur along the interface between the matrix and fibers. Instead, it involves the direct separation of the fibers themselves [60], as illustrated in Fig. 18. In the propagation process, cracks extend directly through the fibers, which could be attributed to the high strength of the matrix material. Ultimately, the failure mechanism involves the direct pulling apart of the fibers. From Fig. 19, it can be seen that there are no multiple peaks in the stress-displacement curve, indicating that the vast majority of samples do not exhibit multiple cracks. In the experiment, it was observed that when the first crack initially appeared, the specimen gradually expanded along that crack, ultimately leading to its final failure. While

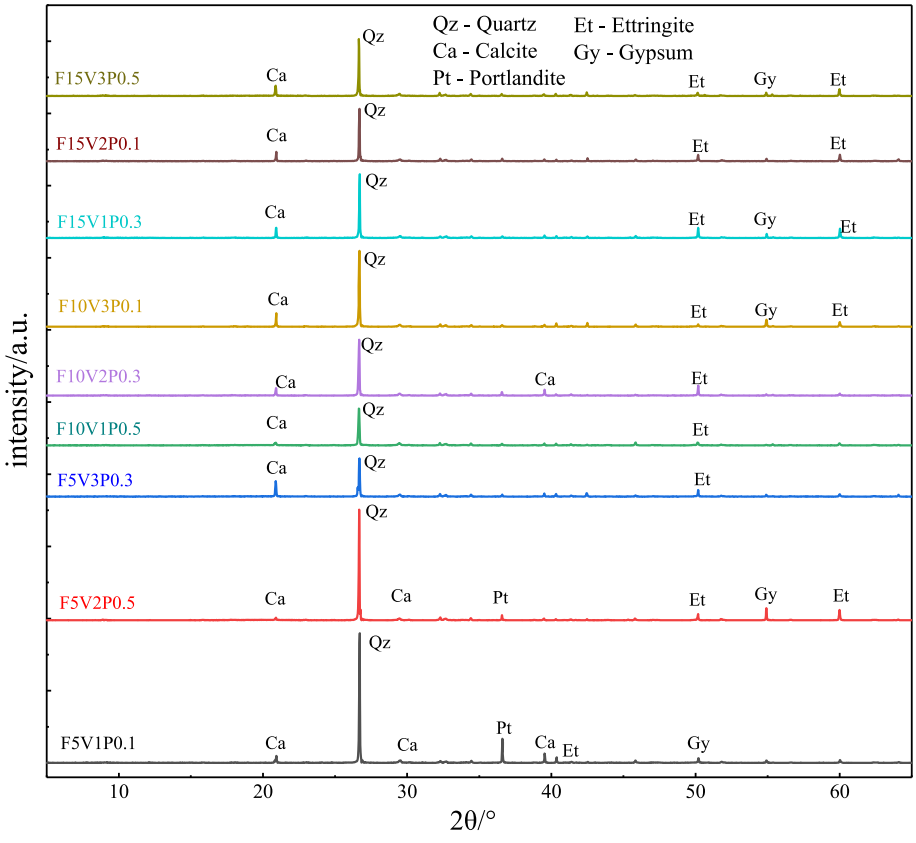


**Fig. 15.** XRD patterns of samples with different proportion.

**Fig. 16.** Pipe spraying effect.

there are no instances of multiple crack propagation, the presence of PVA fibers, owing to their low density and significant quantity within the mortar, effectively inhibits crack development during the continuous cracking process [61]. This results in both improved strength and toughness. Based on this material, our team has improved a high ductility ECC material. Additionally, one of the authors is currently preparing an additional research paper.

To verify the thermal stability of the optimal material, TG-DTA testing was conducted on the material. Qualitatively, the DTA curves show that there are no differences in mortar decomposition temperatures, which are 35–200 °C and 400–500 °C. Endothermic peaks occurred at approximate temperatures 92 °C and 431 °C. The thermogravimetric curves (TG) of F10V1P0.5 mortars are presented in Fig. 20. Throughout the temperature range of the analysis, there was a

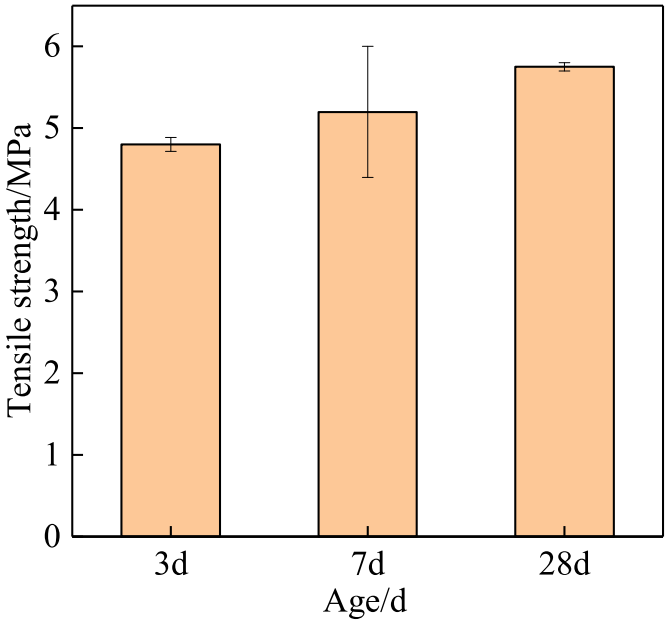


**Fig. 17.** Tensile strength at different ages.

**Fig. 18.** Fracture surface diagram of the specimen.

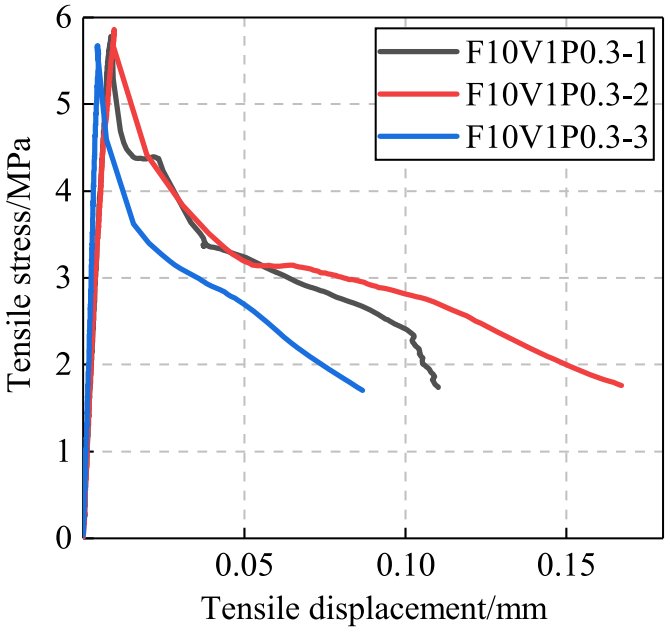


**Fig. 19.** Direct tensile test results.

decrease in weight, and when it reached 900, the weight reduction almost stabilized. The weight loss of materials mainly comes from the combined water decomposed by calcium hydroxide ($Ca(OH)_2$) and the volatile carbon dioxide ($CO_2$) decomposed by calcium carbonate ($CaCO_3$) at high temperatures [62]. From Fig. 20, it can also be seen that there are two main endothermic peaks during the sample heating process, with water evaporation at 35–200 °C and carbonate phase at approximately 400–500 °C [63,64]. Overall, the material lost 10%–11% of its mass.

### 3.6. Properties of PFCM after acid-corrosion

Fig. 21 shows the surface degradation of mortar soaked in a pH = 2 sulfuric acid solution for 0, 3, 7, 28, 56, 112, and 180 days. It can be seen that the degree of surface corrosion increases with time, but there is no significant damage or detachment. After rinsing off the surface floating layer with clean water, it can be observed that there is almost no significant change on the surface of the specimens after 3 days. After 7 days, a layer of transparent film like substance is formed on the surface of the sample with small holes. After 28 days, the specimen showed many small pores, with white crystalline substances embedded in the pores and the corroded surface showing a yellowish brown color. According to previous studies [65,66], after the surface of the specimen reacts with acid, the product of cement hydration product calcium hydrate ferrite decomposition produces ferric hydroxide, resulting in yellowish brown surface. More than 28 days later, a large number of white crystals appeared on the surface of the specimen, which may be caused by the formation of gypsum phase [67]. This indicates that sulfuric acid corrosion of the specimen is a continuous accumulation process, and the alkaline substance in the mortar reacts with sulfuric acid to form a gypsum substance. Because sulfuric acid solution is directly in contact with the surface of the specimen, the corrosion basically occurs on the surface of the specimen. The material has a dense structure, and the internal intrusion of sulfuric acid solution is very small, and white crystals are adhered to the surface of the specimen.

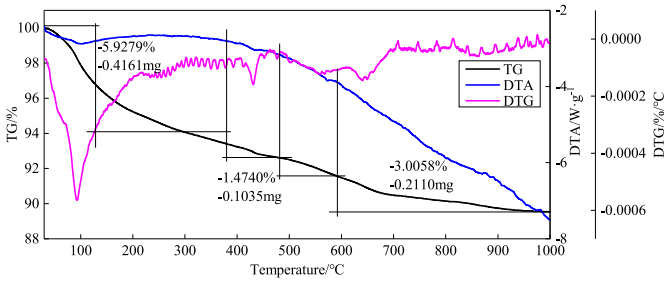


**Fig. 20.** TG,DTA and DTG curves obtained from group F10V1P0.5 in 35–1000 °C temperatures range.

As shown in Fig. 22, the mortar soaked in sulfuric acid solution with pH = 2 showed different degrees of mass loss for different soaking times. When calculating mass loss, the mass loss of three parallel specimens was taken into account to reduce the test error. At the early stage of soaking, the mass of the specimen increased slightly, probably because the sulfuric acid solution penetrated into the internal pores and was absorbed by the mortar. Izquierdo et al. [68] showed through research that after the reaction of mortar and acid solution, the erosion products were deposited, resulting in a denser material structure and further increasing the early mass. The mass loss rate increases with the increase of sulfuric acid solution soaking time. The mass loss rates of 28 days, 56 days, 112 days and 180 days were 0.42%, 1.35%, 3.67% and 4.45%, respectively. After 180 days of soaking, the mortar still showed a good quality retention rate, and the mass loss was only 4.45%. It can also be seen from Fig. 22 that the corrosion depth gradually increases with the passage of soaking time, but gradually slows down, and the corrosion depth increases rapidly in the initial stage of soaking. In 56 days, the corrosion depth reaches 0.4 mm, which is 69% of the corrosion depth reached at 180 days.

According to equation (1), the flexural strength ratio of specimens soaked in sulfuric acid solution was calculated [69], as shown in Fig. 23. It can be seen that the flexural strength increases with the extension of soaking time, but the change in strength gradually slows down after the corrosion age is greater than 28 days.

$$R_S = \frac{R_b - R_h}{R_b} \tag{1}$$

$R_S$—— Flexural strength ratio of specimens soaked in acid;
$R_b$—— Standard curing 28d specimen flexural strength, MPa;
$R_h$—— Flexural strength of specimen after soaking in acid, MPa。

It can also be seen from Fig. 23 that with the extension of soaking time, the flexural corrosion resistance coefficient gradually decreases, indicating that the corrosion of the sample is becoming more and more serious. In the early stage of soaking, the flexural corrosion resistance coefficient decreases rapidly, and the change is small in the later stage, indicating that the corrosion is more obvious in the early stage, but the flexural corrosion resistance coefficient $K$ is greater than 0.8, according to the national standard GB/T 749–2008 [69]. The corrosion resistance coefficient $K > 0.8$ of the specimen after six months of corrosion is qualified, so this material meets the current national standard.

By conducting impermeability tests and chloride ion permeability tests, it was found that when the permeability pressure reached 4 MPa, there was still no water seepage on the surface of the PFCM, and the effective diffusion coefficient of chloride ions was $0.1 \times 10^{-12}$ $m^2/s$, referring to the evaluation standard for concrete permeability [70], the permeability level of chloride ion diffusion coefficient is Grade V, less than $0.5 \times 10^{-12}$ $m^2/s$, with extremely low permeability. This may be due to the fact that the redispersible polymer powder in the material is wrapped outside the hydration product, increasing the thickness of the external hydration film, preventing the penetration of water molecules, and effectively improving the permeability of the mortar material. On the other hand, good impermeability indicates that the material is dense, thereby enhancing its corrosion resistance.

In this study, cumulative porosity and pore size distribution were measured to estimate the total porosity and pore structure of mortar samples before and after sulfuric acid corrosion (Fig. 24). From Fig. 24, it can be seen that the average pore radius of mortar ranges from 7 nm to

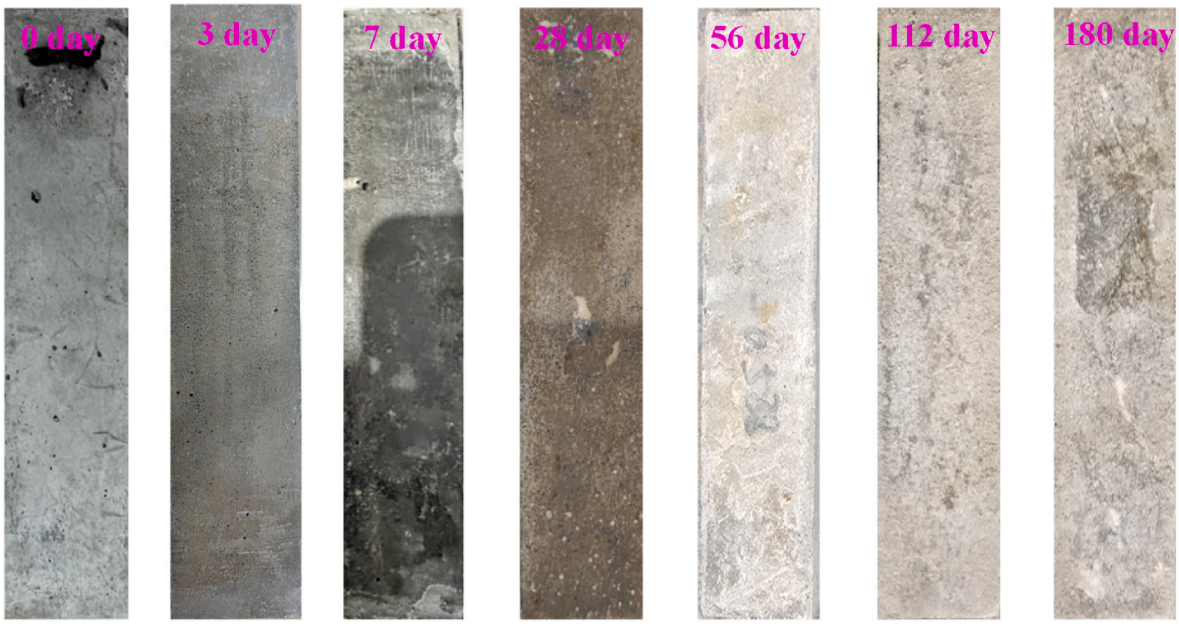


**Fig. 21.** Corrosion surface changes after 0–180 days of sulfuric acid erosion.

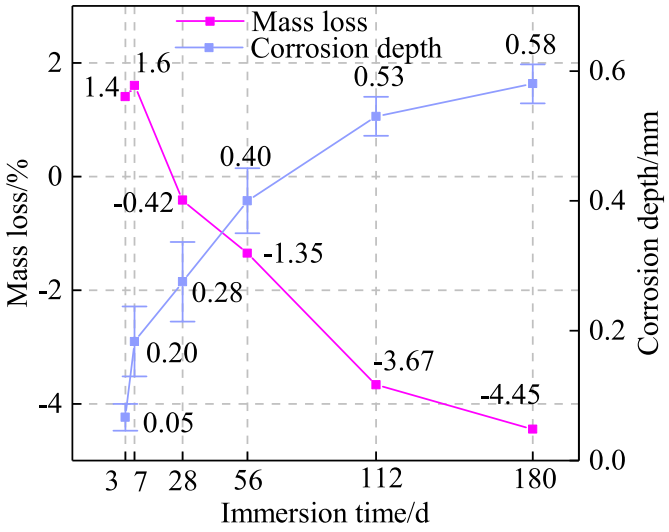


**Fig. 22.** Mass loss rate of specimens immersed in sulfuric acid.

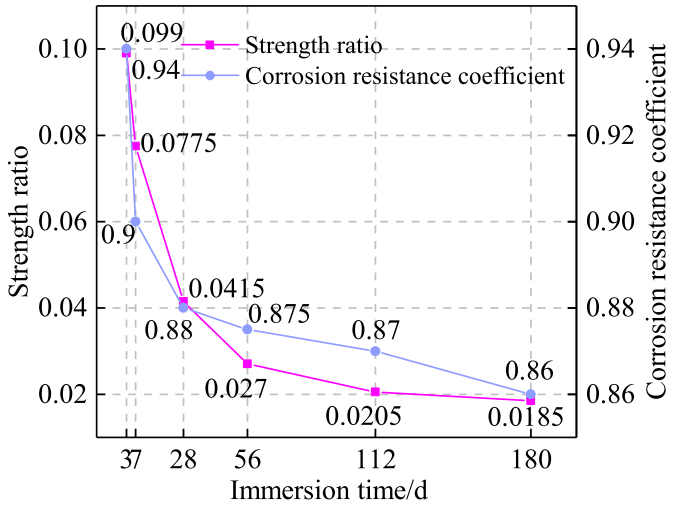


**Fig. 23.** The strength ratio and flexural corrosion resistance coefficient of specimens immersed in sulfuric acid.

500 μm. In general, according to the existing literature [71,72], the pores in cement mortar can be divided into three types, the first type is gel pore (harmless pore), the diameter is less than 0.05 μm, the second type is micropores with a diameter of 0.05 μm–0.1 μm, less harmful pores, the third is large pore, the diameter is greater than 0.1 μm harmful pore. The pores of harmful pores are less, mainly focus on micropores. The total porosity of all samples increases with age, and the total porosity of mortar increases from about 0.04 mL/g to 0.07 mL/g. In particular, after 180 days of corrosion, the porosity in the pore size range of 10 nm–100nm was lower than that in the pore size range of 112 days, but the porosity in the pore size range of 180 days (0.01–1 μm) was the largest. This indicates that many harmful pores are only induced after a corrosion cycle of up to 112 days. At 180 days of corrosion, the total porosity is 1.75 times that of uncorroded.

Fig. 25 shows the XRD spectra of the corrosion products adhered to the surface of the mortar after 180 days of immersion in $H_2SO_4$ solution with a pH of 2, as well as the XRD spectrum of the uncorroded mortar. It is evident that the mortar exposed to the $H_2SO_4$ solution produces an increased amount of gypsum. A comparison of the two XRD patterns reveals significant differences, particularly in the presence of ettringite, calcium carbonate, and gypsum. The formation of gypsum within the corrosion layer is a result of the reaction and deposition of dissolved $Ca^{2+}$ and $SO_4^{2-}$ ions from the solution. Additionally, the diffraction peaks associated with ettringite and calcium silicate either disappear or weaken after exposure to the acid, indicating their complete or partial dissolution, which is consistent with the results of Jia et al. [73].

## 4. Conclusions

A high-strength and durability spraying material was studied for the complex service environment of pipelines, and the following conclusions were obtained:

(1) The optimal material was obtained through orthogonal experiments, with an early compressive strength of 80 MPa and a flexural strength of 16 MPa. By analyzing the range and variance

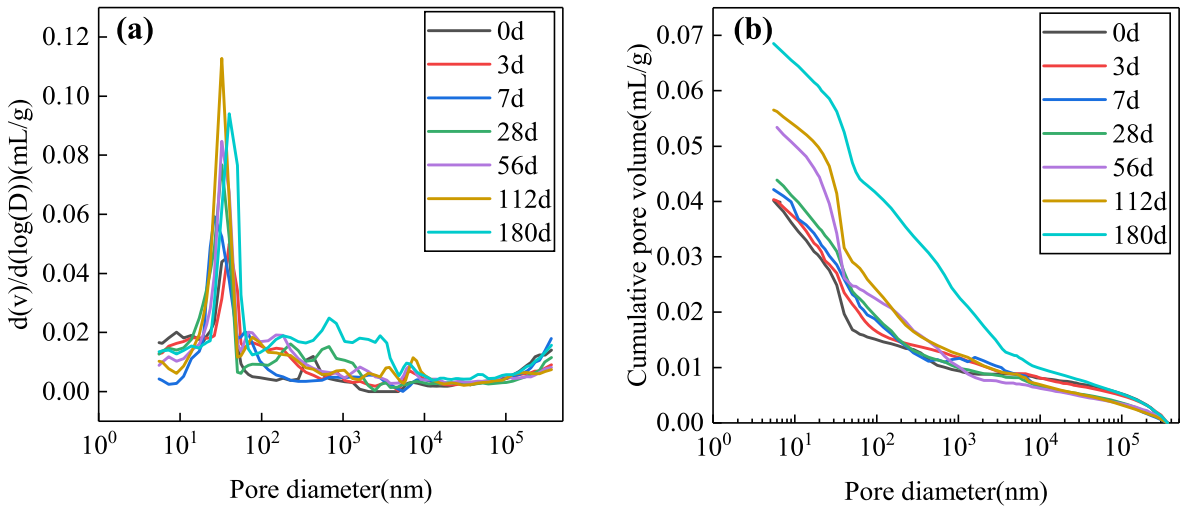


**Fig. 24.** Pore size distribution of sprayed mortar with different corrosion cycles. (a) The content of pores with different diameter and (b) accumulated pore volume.

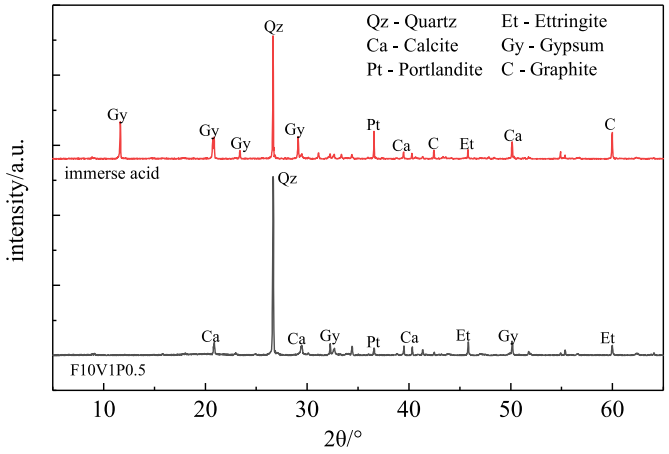


**Fig. 25.** XRD patterns of non-acid corroded and acid corroded powders mixture.

of the orthogonal experimental results of materials, the influencing factors weights on setting time and fluidity were consistent, ranging from large to small: fly ash > PVA fiber > redispersible polymer powder. The influencing factors weights on compressive strength ranged from large to small: redispersible polymer powder > fly ash > PVA fiber, and the influencing factors weights on flexural strength ranged from large to small: fly ash > redispersible polymer powder > PVA fiber.

(2) The optimal ratio obtained by the test was 10% fly ash, 1% redispersible polymer powder and 0.5% PVA fiber. Its initial setting time is 60 min, final setting time is 180min, fluidity is 175 mm, 28d compressive strength is 102.5 MPa, flexural strength is 20 MPa, and tensile strength is 5.16 MPa.

(3) The optimal material was subjected to impermeability tests, chloride ion penetration tests, and sulfuric acid corrosion tests. The impermeability strength reached 4 MPa, the chloride ion diffusion coefficient was less than 0.1 × $10^{-12}$ $m^2/s$, and the permeability was V grade, indicating extremely low permeability. In an acid solution, the mass loss rate increases with the increase of sulfuric acid solution soaking time. The mass loss rates of 28 days, 56 days, 112 days and 180 days were 0.42%, 1.35%, 3.67% and 4.45%, respectively. After 180 days of soaking, the mortar still showed a good quality retention rate, and the mass loss was only 4.45%. The flexural corrosion resistance coefficient *K* is greater than 0.8, this material meets the current national standard.

(4) Microscopic tests such as XRD, MIP, and TG-DTA were conducted on the material to demonstrate its acid corrosion resistance and thermal stability. The XRD test results of the acid corroded sample showed that gypsum is the main degradation product under the action of sulfuric acid.

## Declaration of competing interest

The authors declare that they have no known competing financial interests or personal relationships that could have appeared to influence the work reported in this paper; the work described has not been published before; that it is not under consideration for publication anywhere else; that its publication has been approved by all co-authors; that there is no conflict of interest regarding the publication of this article.

## Acknowledgement

The authors are grateful for the financial support from National Key Research and Development Program of China (No.2022YFC3801000), National Natural Science Foundation of China (No.52278378), Key Specialized Research and Development Breakthrough in Henan Province (No. 232102321073, 232102321074), Scientific and technological research project in Henan province (No.232300421066), Postdoctoral Research Foundation of China (2022M722883, 2022M722884), the Program for Science and Technology Innovation Talents in Universities of Henan Province (No. 23HASTIT007).

## References

[1] Chung KL, Song C, Li Y, Zhang C. Correlation between microwave properties and compressive strength of engineered cementitious mortar. Microw Opt Technol Lett 2016;58:2696–9.
[2] Brandt AM. Fibre reinforced cement-based (FRC) composites after over 40 years of development in building and civil engineering. Compos Struct 2008;86:3–9.
[3] Zhang P, Li D, Qiao Y, Zhang S, Sun C, Zhao T. Effect of air entrainment on the mechanical properties, chloride migration, and microstructure of ordinary concrete and fly ash concrete. J Mater Civ Eng 2018;30:4018265.
[4] Jiang C, Jiang L, Tang X, Gong J, Chu H. Impact of calcium leaching on mechanical and physical behaviors of high belite cement pastes. Construct Build Mater 2021;286:122983.
[5] Yuan S. Discussion on anti-seepage technologies in the construction of small-scale rural water conservancy projects. J World Architecture 2022;6:19–24.
[6] Luo X, Xu J, Bai E, Li W. Mechanical properties of ceramics–cement based porous material under impact loading. Mater Des 2014;55:778–84.
[7] Neubauer CM, Jennings HM, Garboczi EJ. Mapping drying shrinkage deformations in cement-based materials. Cement Concertr Res 1997;27:1603–12.

[8] Jia G, Li Z, Liu P, Jing Q. Applications of aerogel in cement-based thermal insulation materials: an overview. Mag Concr Res 2018;70:822–37.
[9] Ogura H, Nerella VN, Mechtcherine V. Developing and testing of strain-hardening cement-based composites (SHCC) in the context of 3D-printing. Materials 2018;11:1375.
[10] Tao Y, Lesage K, Van Tittelboom K, Yuan Y, De Schutter G. Influence of aluminum sulfate on mobility and adhesion of hydroxyethyl methyl cellulose in cement-based materials for tunnel linings. Cement Concr Compos 2022;131:104594.
[11] Li G, Shi X, Gao Y, Ning J, Chen W, Wei X, Wang J, Yang S. Reinforcing effects of carbon nanotubes on cement-based grouting materials under dynamic impact loading. Construct Build Mater 2023;382:131083.
[12] Shu X, Zhao Y, Liu Z, Zhao C. A study on the mix proportion of fiber-polymer composite reinforced cement-based grouting material. Construct Build Mater 2022;328:127025.
[13] Jiang D, Cui S, Xu F, Tuo T. Impact of leaf fibre modification methods on compatibility between leaf fibres and cement-based materials. Construct Build Mater 2015;94:502–12.
[14] Pan T, Teng H, Liao H, Jiang Y, Qian C, Wang Y. Effect of shaping plate apparatus on mechanical properties of 3D printed cement-based materials: experimental and numerical studies. Cement Concertr Res 2022;155:106785.
[15] Yang R, He T, Guan M, Guo X, Xu Y, Xu R, Da Y. Preparation and accelerating mechanism of aluminum sulfate-based alkali-free accelerating additive for sprayed concrete. Construct Build Mater 2020;234:117334.
[16] Zhou Z, Shen Y, Hao J, Bai Z, Liu Y, Kou H. Inexpensive anti-icing concrete material for application to tunnel and slope engineering infrastructures in cold regions. ACS Applied Materials \& Interfaces 2021;13:53030.
[17] Camargo-P E Rez NR, A N-Garc I A Jin Abell, Fuentes L. Use of rice husk ash as a supplementary cementitious material in concrete mix for road pavements. J Mater Research and Technol 2023;25:6167–82.
[18] Holter KG, Smeplass S, Jacobsen S. Freeze–thaw resistance of sprayed concrete in tunnel linings. Mater Struct 2016;49:3075–93.
[19] Zhu H, Wang T, Wang Y, Li VC. Trenchless rehabilitation for concrete pipelines of water infrastructure: a review from the structural perspective. Cement and Concrete Composites 2021;123:104193.
[20] Zhang X, Fang H, Shi M, Du M, Yang K, Li B, Zhang Z. Structural performance of corroded concrete pipes after mortar spraying rehabilitation under traffic load. Tunn Undergr Sp Tech 2022;128:104620.
[21] Zhao Y, Ma B, Ariaratnam ST, Zeng C, Yan X, Wang F, Wang T, Zhu Z, He C, Shi G. Others. Structural performance of damaged rigid pipe rehabilitated by centrifugal spray on mortar liner. Tunn Undergr Sp Tech 2021;116:104117.
[22] Zhang X, Fang H, Hu Q, Ma B, Hu S, Du M, Du X, Yang K, Li B, Shi M. Mechanical performance of corroded reinforced concrete pipelines rehabilitated with sprayed-on cementitious liners subjected to combined loads. Tunn Undergr Sp Tech 2022;120:104266.
[23] Motlagh SG, Jain A, Najafi M. Comparison of spray-on linings for water pipeline renewal applications. Pipelines. Pipelines and Trenchless Construction and Renewals—A Global Perspective 2013:1113. 2013.
[24] Royer JR. Geopolymer lining of corroded reinforced concrete sanitary sewer pipes. NACE; 2019. p. 2019.
[25] Du G, Kong Q, Wu F, Ruan J, Song G. An experimental feasibility study of pipeline corrosion pit detection using a piezoceramic time reversal mirror. Smart Mater Struct 2016;25:37002.
[26] Li P, Wang F, Gao J, Lin D, Gao J, Lu J, et al. Failure mode and the prevention and control technology of buried PE pipeline in service: state of the art and perspectives. Adv Civ Eng 2022;2022:2228690.
[27] Nazar S, Yang J, Amin MN, Husnain M, Ahmad F, Alabduljabbar H, Deifalla AF. Investigating the influence of PVA and PP fibers on the mechanical, durability, and microstructural properties of one-Part Alkali-activated mortar: an experimental study. Journal of Materials Research and Technology 2023;25:3482–95.
[28] Zhao D, Wang F, Liu P, Hu S, Hu C, Yang L. Enhanced mechanical properties of polymer-modified cementitious materials via organosilane fly ash hybrid–polyvinyl pyrrolidone crosslink network. Constr Build Mater 2022;330:127119.
[29] Bel L GO, Bos CEM, Schwaiger R, Flohr A, Osburg A. Micromechanics-based investigation of the elastic properties of polymer-modified cementitious materials using nanoindentation and semi-analytical modeling. Cement and Concrete Composites 2018;88:100–14.
[30] Ryu GS, Koh KT, Kang ST, Park JJ. Mechanical properties of ductile fiber reinforced cementitious composites for rehabilitation on concrete structures. Key Eng Mater 2008;385-387:697–700.
[31] Mishra G, Warda A, Shah SP. Carbon sequestration in graphene oxide modified cementitious system. J Build Eng 2022;62:105356.
[32] El-Helou RG, Koutromanos I, Moen CD, Moharrami M. Triaxial constitutive law for ultra-high-performance concrete and other fiber-reinforced cementitious materials. J Eng Mech 2020;146:4020062.
[33] Wang J, Xu Y, Wu X, Zhang P, Hu S. Advances of graphene-and graphene oxide-modified cementitious materials. Nanotechnol Rev 2020;9:465–77.
[34] Guan X, Yu L, Li H. Experimental study on fracture mechanics of cementitious materials reinforced by graphene oxide–silica nanocomposites. Constr Build Mater 2022;325:126758.
[35] Luo J, Zhu G, Zhang F, Li Q, Zhao T. Orthogonal experimentation for optimization of TiO2 nanoparticles hydrothermal synthesis and photocatalytic property of a TiO2/concrete composite. Rsc Adv 2015;5:6071–8.
[36] Verma MKS. Effect of parameters on adhesion strength for slurry spray coating technique. Mater Manuf Process 2017;32:416–24.
[37] Astm A, Others. Standard specification for flow table for use in tests of hydraulic cement. ASTM West Conshohocken; 2014. p. 1.
[38] Standard for test method of performance on building mortar. 2009. 70-2009.
[39] Choi SJ, Lee SS, Monteiro PJ. Effect of fly ash fineness on temperature rise, setting, and strength development of mortar. J Mater Civil Eng 2012;24:499–505.
[40] Tong L, Pan S, Qiu Y, Xuan G, Liu S. Experimental research on grouting material with large volume fly ash. Dongnan Daxue Xuebao/Journal of Southeast University (Natural Science Edition) 2002;32:643.
[41] Nan X, Ji J, Yang X, Chen G, Li M, Tang W. Frost resistance of redispersible polymer powder–modified fast-hardening cement mortars under simulated climatic conditions. J Mater Civil Eng 2023;35:4023245.
[42] Lu H, Dong Q, Yan S, Chen X, Wang X. Development of flexible grouting material for cement-stabilized macadam base using response surface and genetic algorithm optimization methodologies. Constr Build Mater 2023;409:133823.
[43] Li G, Wu X. Influence of fly ash and its mean particle size on certain engineering properties of cement composite mortars. Cement Concertr Res 2005;35:1128–34.
[44] Zhao B, Liu YS, He SH, Zhang Y. The effects of basalt fiber parameter on the fluidity of the cement mortar. Journal of Wuhan University of Technology 2009;31:5–8.
[45] Phan V. Relationship between the adhesive properties and the rheological behavior of fresh mortars. Ecole normale superieure de Cachan-ENS Cachan; 2012.
[46] Chung KL, Ghannam M, Zhang C. Effect of specimen shapes on compressive strength of engineered cementitious composites (ECCs) with different values of water-to-binder ratio and PVA fiber. Arabian Journal for Science & Engineering 2017;43:1825–37.
[47] Li Y, Liu ZJ. Behavior of high performance PVA fiber reinforced cement composites under uniaxial compressive load. Applied Mechanics and Materials 2012;174:687–91.
[48] Sun Y, Wang KQ, Lee HS. Prediction of compressive strength development for blended cement mortar considering fly ash fineness and replacement ratio. Constr Build Mater 2021;271:121532.
[49] Ye ZM, Chen W, Cheng X. Impermeability of Sulphoaluminate cement mortar modified by redispersible polymer powders. Advanced Materials Research 2011;168:1886–90.
[50] Unal M, Simsek O. Determination of optimum fly ash and PVA fiber ratio in cement mortars. J Polytech 2022;25:477–89.
[51] Du P, Zhou ZH, Ye ZM, Cheng X. Redispersible polymer powder-modified sulphoaluminate cement mortar. Key Engineering Materials 2017;726:495–9.
[52] Liu LP, He Y, He LP, Tan H. Mechanical properties of fly ash-based geopolymer/cement composites. J Wuhan Univ Technol 2015;37:9–12.
[53] Lee J. Physical properties of polymer-modified cement mortars by the functional additives and modification of polymerization. J Ceram Process Res 2017;18:220–9.
[54] Kaya M, K O Ksal F. Influences of high temperature on mechanical properties of fly ash based geopolymer mortars reinforced with PVA fiber. Revista de la construccion 2021;20:393–406.
[55] Zuo X, Wang J, Sun W, Li H, Yin G. Numerical investigation on gypsum and ettringite formation in cement pastes subjected to sulfate attack. Computers and Concrete, An International Journal 2017;19:19–31.
[56] Yang R, Buenfeld NR. Microstructural identification of thaumasite in concrete by backscattered electron imaging at low vacuum. Cement Concertr Res 2000;30:775–9.
[57] Clark BA, Brown PW. Formation of ettringite from monosubstituted calcium sulfoaluminate hydrate and gypsum. J Am Ceram Soc 1999;82:2900–5.
[58] Hu D, Guo Z, Jun T, Yuan C. A Novel Hydrophilic PVA fiber reinforced thermoplastic polyurethane materials for water-lubricated stern bearing. Fober Polym 2021;22:171–83.
[59] Surin VI, Polskij VI, Osintsev AV, Dzhumaev PS. Applying scanning contact potentiometry for monitoring incipient cracks in steels. Russ J Nondestruct + 2019;55:59–67.
[60] Li Z, Sheikh MN, Feng H, Hadi MN. Mechanical properties of ambient cured fly ash-slag-based engineered geopolymer composites with different types of fibers. Struct Concrete 2023;24:2363–83.
[61] Xiao S, Cai Y, Guo Y, Lin J, Liu G, Lan X, Song Y. Experimental study on axial compressive performance of polyvinyl alcohol fibers reinforced fly ash—slag geopolymer composites. Polymers-basel 2021;14:142.
[62] Park WJ, Lee HS, Park KB. A study on the development mechanism of early strength in cement mortar using an early-strength polycarboxylated agent. Key Engineering Materials 2007;348:473–6.
[63] Andrade F, Pires T, Silva J. Influence of silicon-dioxide nanoparticles in cementitious mortars: verification using x-ray diffraction, thermal analysis, physical, and mechanical tests. Mater Res Express 2023;10:25004.
[64] Kim MS, Jun Y, Lee C, Oh JE. Use of CaO as an activator for producing a price-competitive non-cement structural binder using ground granulated blast furnace slag. Cement Concertr Res 2013;54:208–14.
[65] Hu X, Hou X, Long T, Tao X, Liu F, Xiao B. Analysis for composition change on acid rain attacking hydrated cement past. Journal of Railway Science and Engineering 2007;4:47–51.
[66] Wang K, Ma B, Long S. Microanalysis of the change of phase compositions of hardened cement paste in response to acid rain attack. Journal of the Chinese Ceramic Society 2009;37:880–4.
[67] Messaoudene I, Ezziane M, Molez L. Durability of Portland cements composed of industrial waste fillers in an acidic environment. J Mater Eng Struc 2019;6:383–95.
[68] Izquierdo S, Rodr I Guez E, de Guti E, Rrez RMIA. Resistance to acid corrosion of blended cements mortars with spent fluid catalytic cracking (sFCC) catalyst. Rev Ing Constr 2015;30:169–76.
[69] GB/T 749-2008 Test method for determing capability of resisting sulfate corrode of cement. 2008.
[70] Society SOCC. Guide to durability design and construction of concrete structures. 2004. CCES01-2004.

[71] Liu X, Liu L, Lyu K, Li T, Zhao P, Liu R, Zuo J, Fu F, Shah SP. Enhanced early hydration and mechanical properties of cement-based materials with recycled concrete powder modified by nano-silica. J Build Eng 2022;50:104175.
[72] Pang B, Zhou Z, Xu H. Utilization of carbonated and granulated steel slag aggregate in concrete. Constr Build Mater 2015;84:454–67.
[73] Xiao J, Zhou SQ. Effect of low-calcium fly ash on the resistance of cement mortar to sulfate attack in the form of acid rain. Key Engineering Materials 2005;302:84–90.